Suppression of Electron Temperature Gradient Turbulence via Negative Magnetic Shear in NSTX

H. Y. Yuh,[1,*] S. M. Kaye,[2] F. M. Levinton,[1] E. Mazzucato,[2] D. R. Mikkelsen,[2] D. R. Smith,[3] R. E. Bell,[2] J. C. Hosea,[2] B. P. LeBlanc,[2] J. L. Peterson,[2] H. K. Park,[4] and W. Lee[4]

[1]*Nova Photonics Inc., Princeton, New Jersey 08540, USA*
[2]*Princeton Plasma Physics Laboratory, Princeton University, Princeton, New Jersey 08543, USA*
[3]*Department of Engineering Physics, University of Wisconsin-Madison, Madison, Wisconsin 53706, USA*
[4]*POSTECH, Pohang 790-784, Korea*

(Received 2 July 2010; published 3 February 2011)

Negative magnetic shear is found to suppress electron turbulence and improve electron thermal transport for plasmas in the National Spherical Torus Experiment (NSTX). Sufficiently negative magnetic shear results in a transition out of a stiff profile regime. Density fluctuation measurements from high-k microwave scattering are verified to be the electron temperature gradient (ETG) mode by matching measured rest frequency and linear growth rate to gyrokinetic calculations. Fluctuation suppression under negligible $\mathbf{E} \times \mathbf{B}$ shear conditions confirm that negative magnetic shear alone is sufficient for ETG suppression. Measured electron temperature gradients can significantly exceed ETG critical gradients with ETG mode activity reduced to intermittent bursts, while electron thermal diffusivity improves to below 0.1 electron gyro-Bohms.

DOI: 10.1103/PhysRevLett.106.055003 PACS numbers: 52.55.Fa

Understanding and ameliorating anomalous electron thermal transport is crucial for magnetically confined fusion reactors. In the National Spherical Torus Experiment (NSTX), electron thermal transport can be the dominant loss channel when ion temperature gradient microinstabilities are stabilized by strong $\mathbf{E} \times \mathbf{B}$ shear. Previous works have associated improved confinement with reversed shear, or negative magnetic shear, $s \equiv (r/q)dq/dr$ [1–5]. In this work, we present evidence that electron temperature gradient (ETG) microinstability suppression by reversed magnetic shear is responsible for improving electron thermal confinement in internal transport barriers (e ITBs).

Two sets of L-mode discharges are used for this study, both at a toroidal field of 0.55 T. One set of neutral beam plus high harmonic fast wave (HHFW) rf heated discharges used 1 MA of plasma current while the other used rf only at 600 kA, with deuterium or helium as the bulk plasma species in both scenarios. Strong statistical correlations between kinetic profile features such as the location of magnetic shear minima and electron temperature gradient maxima have been reported in [6].

The reduction of high average amplitude high-k activity to infrequent short-duration bursts improves electron confinement in the strongly negative magnetic shear region. Figures 1(a)–1(c) compare a discharge with an e ITB during the reversed-shear phase of the discharge (0.17–0.27 s) to an identically heated discharge in Figs. 1(d)–1(f) with a monotonic q profile. Electron density fluctuations, shown as the black trace in Figs. 1(a) and 1(d), are measured at electron gyroscale wave numbers ($k_\perp \rho_e \leq 0.6$) by the high-k collective microwave scattering diagnostic [7,8]. The red traces with error bars using the right-hand axis in Fig. 1(a) show that, despite maintaining a normalized inverse electron temperature gradient scale length above the GS2 calculated critical ETG value ($R/L_{T_e,\mathrm{crit}} \approx 18$), one observes only short-duration bursts of high-k fluctuations. The normal shear plasma in Fig. 1(d), despite reaching a higher central temperature, does not exceed the ETG critical gradient ($R/L_{T_e,\mathrm{crit}} \approx 12$) due to the onset of sustained high-k activity near the critical gradient.

The reversed-shear phase of Fig. 1(a) ends with a rapid collapse of central q due to a short-duration MHD reconnection event, triggering a series of high-k bursts and a simultaneous sharp decrease in R/L_{T_e}. Electron temperature profiles are shown in Fig. 1(b) with labels corresponding to three times in Fig. 1(a): (1) during the e ITB, (2) shortly after the current redistribution, and (3) the reheat period with a monotonic q profile. Although it is difficult to separate MHD and microturbulence effects in causing the decline of the central temperature, after transitioning to normal shear and with no further MHD activity, only lower temperature gradients are observed at the same heating power with an increase in the high-k density fluctuation amplitude.

Mazzucato *et al.* [9] have previously identified measured high-k fluctuations as ETG by comparing the gradients for fluctuation onset against linear stability calculations. Here, the rest frequency of an active, high-amplitude mode in the absence of an e ITB has been calculated by fitting peak amplitude frequencies from a time series of high-k spectra as a function of plasma toroidal rotation. This method avoids large uncertainties in k_θ from ray-tracing calculations. The rest frequency for a test case was found to be 630 ± 50 kHz in the electron direction while GS2

 © 2011 American Physical Society

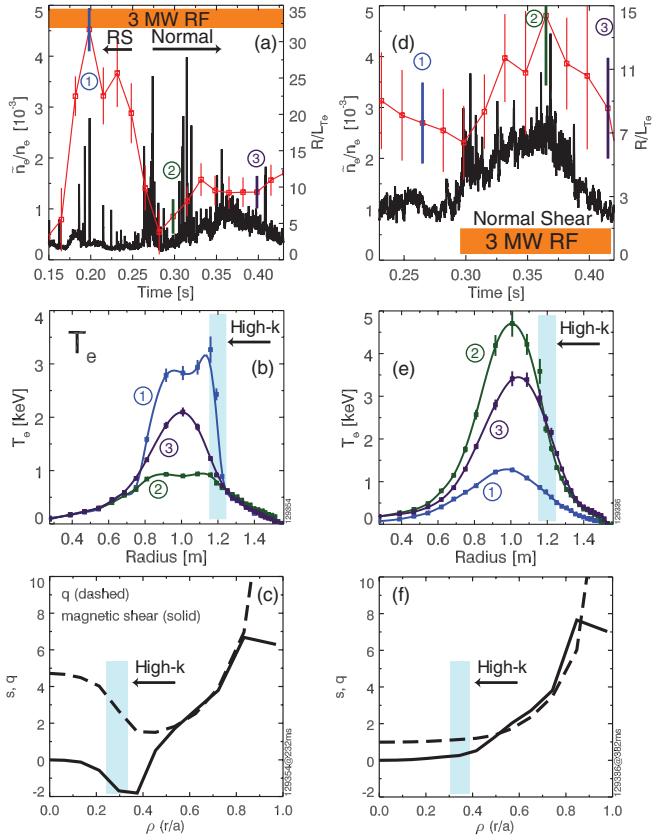

FIG. 1 (color). A comparison of high-k turbulence between a reversed-shear (RS) (a)–(c) and normal shear (d)–(f) discharges. Panels (a) and (d) show as a function of time normalized $\tilde{n}_e/n_e$ density fluctuations measured by the high-k diagnostic and normalized inverse electron temperature gradient scale length, R/L_{T_e}, in red using the right-hand axis. T_e profiles in (b) and (e) are labeled by numbers corresponding to times in (a) and (d) and shows the measurement region for the high-k fluctuations. Panels (c) and (f) show q and magnetic shear profiles of interest for each discharge.

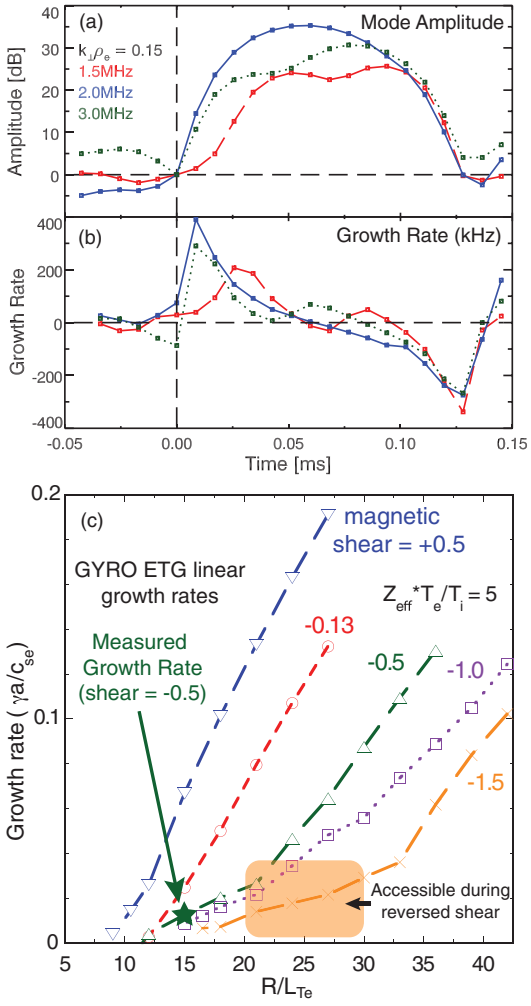

FIG. 2 (color). (a) Time resolved mode amplitude of an ETG burst at three frequencies. (b) Growth rate corresponding to mode amplitudes. (c) GYRO computed growth rates, showing sensitivities to variations in magnetic shear and R/L_{T_e}. Star indicates measured growth rate at $s = -0.5$.

calculates the rest frequency to be 500 ± 90 kHz for matching plasma conditions. The range for the GS2 calculation accounts for input uncertainties in wave number and electron temperature gradient. A caveat for this comparison is that the rest frequency measurement is made for the peak amplitude mode, while linear calculations provide values for the fastest growing mode.

The growth rate of an ETG burst, shown in Fig. 2(b), is calculated from time derivatives of the mode amplitudes, shown in Fig. 2(a), by analyzing high-k spectral data at high time resolution. ETG mode growth occurs at the electron sound speed time scale, substituting electron for ion mass, corresponding to a peak growth rate of 400 kHz, with the mode reaching peak amplitude for this example in approximately 50 μs. The fastest measured growth rate in Fig. 2(b), shown as a star in Fig. 2(c), is found to be consistent with GYRO growth rate calculations at the same value of R/L_{T_e} and magnetic shear.

Bursts of ETG appear to regulate the electron temperature gradient even during reversed-shear discharges with electron transport barriers. Despite being active for only 1.6% of the time during the reversed-shear e ITB period, ETG bursts appear to limit R/L_{T_e} from reaching higher values.

The improvement in electron thermal diffusivity between a negative shear e ITB and typical H-mode confinement as computed by TRANSP is shown in Fig. 3. For the e-ITB cases where ETG remains low, χ_e is found to be reduced over an order of magnitude compared to typical H modes. This is shown in the strongly negative shear case ($s = -1.6$) where χ_e is found to increase only weakly with increasing electron temperature gradient above ETG linear stability. When ETG bursts appear with increased R/L_{T_e}, the time averaged χ_e is modestly increased. This is shown in the ($s = -0.6$) case where bursts appear when R/L_{T_e}

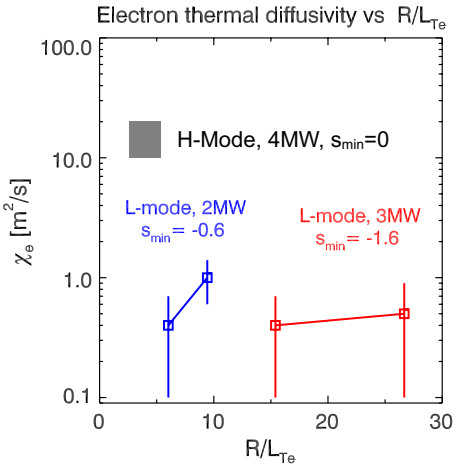

FIG. 3 (color online). TRANSP calculations shows e ITBs have low thermal diffusivities that show a weak dependence to increasing electron temperature gradients above $R/L_{T_e,\mathrm{crit}}$. Results are shown for cases with low observed high-k activity at $\rho = r/a = 0.3$ ($R = 120$ cm).

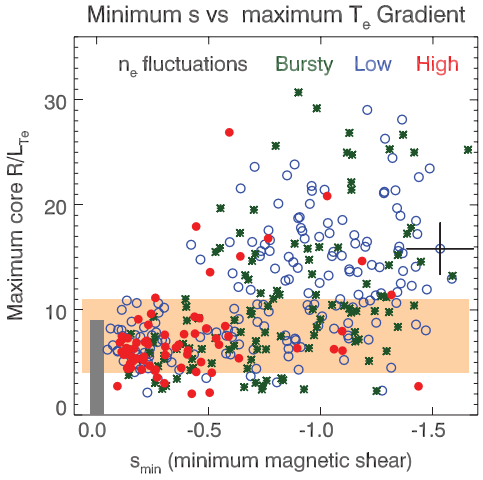

FIG. 4 (color). Value of profile minimum magnetic shear versus peak electron temperature gradient. A transition from stiff profiles to e ITBs is observed at $s_{\mathrm{min}} \leq -0.4$, coincident with reductions in average ETG amplitudes. Horizontal shaded region indicates the range of ETG $R/L_{T_e,\mathrm{crit}}$ calculated using GS2 simulations for a sampling of discharge conditions spanning the data set. Gray vertical bar shows typical H-mode conditions.

increases from 6 to 10. As another example, during the ITB phase in Figs. 1(a)–1(c), $\chi_e = 1$ m^2/s. This result is consistent with earlier nonlinear simulation results from Jenko and Dorland [10]. Their nonlinear simulations using GENE and GS2, although performed for conditions not matching NSTX, also showed highly reduced ETG transport that was weakly sensitive to R/L_{T_e} above $R/L_{T_e,\mathrm{crit}}$ at $s = -1.0$.

Statistical analysis of a collection of discharges further supports that ETG plays a role in limiting the electron temperature gradient. Figure 4 shows that in the zero and weakly negative magnetic shear regime, defined as $s_{\mathrm{min}} \geq -0.4$, the T_e profile is stiff, and high-k measurements show that ETG is often continuously active with a high average amplitude (red closed circles). However, at strongly negative magnetic shears, $s_{\mathrm{min}} < -0.4$, e-ITB formation is observed where ETG is suppressed to low amplitudes (blue open circles) or reduced to short-duration bursts (green asterisks) at $R/L_{T_e} > R/L_{T_e,\mathrm{crit}}$, where the range of $R/L_{T_e,\mathrm{crit}}$ determined by GS2 and GYRO is shown as the horizontal shaded region. $R/L_{T_e,\mathrm{crit}}$ is found to only weakly depend on magnetic shear. Typical monotonic, H-mode core R/L_{T_e} values are shown by the gray vertical band at zero shear.

Discharges used in Fig. 4 span a substantial range of plasma parameters independent of magnetic shear. All profiles included 2 MW of neutral beam heating for motional Stark effect (MSE) diagnostic measurements, but some also received rf heating up to 3 MW. Plasma densities ranged from $1 \times 10^{19} \leq n_e \leq 4 \times 10^{19}$ m^{-3}. Both helium and deuterium were used as the bulk species with $1.1 \leq Z_{\mathrm{eff}} \leq 4$. Wall conditions varied with differing amounts of predeposited lithium and evaporation rates. However, no direct correlation was found between these parameters and the formation of transport barriers, although lower density plasmas favored reversed magnetic shear q profiles.

Significant $\mathbf{E} \times \mathbf{B}$ shear is present for all data in Fig. 4 due to neutral beam injection necessary for MSE measurements. However, Fig. 1 shows high harmonic fast wave heated discharges with 50 ms beam pulses for diagnostic purposes. Consequently, for such discharges the measured $\mathbf{E} \times \mathbf{B}$ shearing rate is zero within uncertainties at the e-ITB location. While previous results have shown that ETG behavior can be sensitive to changes in the $\mathbf{E} \times \mathbf{B}$ shearing rate [11], robust ETG suppression resulting in confinement improvement has only been observed with strongly negative magnetic shear.

ETG suppression presented in this work cannot be explained using linear stability. While $R/L_{T_e,\mathrm{crit}}$ modestly increases with increasingly negative shear, this improvement cannot explain the observed R/L_{T_e} values. Any positive ETG growth rate in Fig. 2(c) should result in saturated ETG turbulence on submillisecond time scales. Therefore, magnetic shear must be suppressing ETG turbulent transport by limiting the nonlinear mode amplitude. Recent simulations show that reverse magnetic shear suppresses most ETG modes to low amplitudes, but some linearly subdominant modes with elevated $R/L_{T_e,\mathrm{crit}}$ near values seen in e-ITB cases can grow to amplitudes that cause transport.

Figure 2(c) shows increases in slope for the negative shear growth rate curves, indicating changes in the fastest growing mode. Linear extrapolation of the steeper segments gives values of $R/L_{T_e,\mathrm{crit}}$ that better correspond to e-ITB values. Further nonlinear simulation is needed to determine the interactions and effects of the entire ETG mode spectrum.

Observed electron transport falls within the range deemed plausible by published ETG simulation results. In previous works from [5,10,12–14], nonlinear gyrokinetic simulations including GENE, GS2, GYRO, PG3EQ, GTS, and GEM have shown significant ETG streamer driven transport. Because of the strong scaling of the electron gyro-Bohm with toroidal field, using the definition found in [14] as $\chi_{e,\mathrm{GB}} = (\rho_e/L_{T_e})\rho_e v_{te}$, ETG-induced electron transport on NSTX could be quite large. While benchmarked simulations from several codes indicate that ETG can produce transport up to $14\chi_{e,\mathrm{GB}}$ [14], the electron transport observed in Figs. 1(d)–1(f) can be accounted for using only 1–2 electron gyro-Bohms at $\chi_{e,\mathrm{GB}} = 11\ \mathrm{m}^2/\mathrm{s}$. Kaye *et al.* [15] have also reported that the transport in many NSTX *H*-mode discharges are within 5–20 electron gyro-Bohms. Using the assumption that all electron transport is caused by ETG bursts, the transport in Figs. 1(a)–1(c) of $\chi_e = 1\ \mathrm{m}^2/\mathrm{s}$ can be accounted for using only $3\text{–}4\chi_{e,\mathrm{GB}}(17.5\ \mathrm{m}^2/\mathrm{s})$ during the bursts.

It is possible that strong negative shear may be suppressing additional microturbulence. Although improved stability for the microtearing mode was cited in [16] as the cause for confinement improvement in reversed-shear discharges, low-k trapped electron modes and microtearing modes were found to be stable for the discharge shown in Figs. 1(a)–1(c). Instead, initial nonlinear simulations show that multiple high-k electron temperature gradient driven modes are suppressed at the measured wave numbers by magnetic shear reversal. Further simulation scans and a synthetic diagnostic matching the window of k space measured by the physical instrument are necessary to understand why bursts are observed, as bursts have so far not been seen in simulations.

In conclusion, negative magnetic shear allows for a transition out of the stiff electron temperature profile regime. Reduced ETG fluctuations are measured temporally and spatially coincident with *e* ITBs, despite electron temperature gradients exceeding ETG critical gradients. Observed electron transport falls within published limits on ETG-induced transport from benchmarked simulations. Additional comparisons with synthetically diagnosed nonlinear simulations are necessary to understand the critical value of magnetic shear, the nonlinear suppression mechanism, and the nature of ETG bursts. These results also demonstrate the importance of developing current profile control tools for future devices.

*hyuh@pppl.gov

[1] F. M. Levinton *et al.*, Phys. Rev. Lett. **75**, 4417 (1995).
[2] L.-G. Eriksson *et al.*, Phys. Rev. Lett. **88**, 145001 (2002).
[3] E. J. Strait *et al.*, Phys. Rev. Lett. **75**, 4421 (1995).
[4] T. Fujita, S. Ide, H. Shirai, M. Kikuchi, O. Naito, Y. Koide, S. Takeji, H. Kubo, and S. Ishida, Phys. Rev. Lett. **78**, 2377 (1997).
[5] E. Mazzucato *et al.*, Nucl. Fusion **49**, 055001 (2009).
[6] H. Y. Yuh *et al.*, Phys. Plasmas **16**, 056120 (2009).
[7] D. R. Smith, E. Mazzucato, T. Munsat, H. Park, D. Johnson, L. Lin, C. W. Domier, M. Johnson, and J. N. C. Luhmann, Rev. Sci. Instrum. **75**, 3840 (2004).
[8] E. Mazzucato, Phys. Plasmas **10**, 753 (2003).
[9] E. Mazzucato *et al.*, Phys. Rev. Lett. **101**, 075001 (2008).
[10] F. Jenko and W. Dorland, Phys. Rev. Lett. **89**, 225001 (2002).
[11] D. R. Smith *et al.*, Phys. Rev. Lett. **102**, 225005 (2009).
[12] W. Dorland, F. Jenko, M. Kotschenreuther, and B. N. Rogers, Phys. Rev. Lett. **85**, 5579 (2000).
[13] F. Jenko, W. Dorland, and G. W. Hammett, Phys. Plasmas **8**, 4096 (2001).
[14] W. M. Nevins *et al.*, Phys. Plasmas **13**, 122306 (2006).
[15] S. Kaye *et al.*, Nucl. Fusion **47**, 499 (2007).
[16] F. M. Levinton *et al.*, Phys. Plasmas **14**, 056119 (2007).